ARTICLES
https://doi.org/10.1038/s41559-022-01774-3

nature ecology & evolution

Check for updates

Enhanced habitat loss of the Himalayan endemic flora driven by warming-forced upslope tree expansion

Xiaoyi Wang[1], Tao Wang[1]✉, Jinfeng Xu[1,2], Zehao Shen[3], Yongping Yang[4], Anping Chen[5], Shaopeng Wang[3], Eryuan Liang[1] and Shilong Piao[1,6]

High-elevation trees cannot always reach the thermal treeline, the potential upper range limit set by growing-season temperature. But delineation of the realized upper range limit of trees and quantification of the drivers, which lead to trees being absent from the treeline, is lacking. Here, we used 30 m resolution satellite tree-cover data, validated by more than 0.7 million visual interpretations from Google Earth images, to map the realized range limit of trees along the Himalaya which harbours one of the world's richest alpine endemic flora. The realized range limit of trees is ~800 m higher in the eastern Himalaya than in the western and central Himalaya. Trees had reached their thermal treeline positions in more than 80% of the cases over eastern Himalaya but are absent from the treeline position in western and central Himalaya, due to anthropogenic disturbance and/or premonsoon drought. By combining projections of the deviation of trees from the treeline position due to regional environmental stresses with warming-induced treeline shift, we predict that trees will migrate upslope by ~140 m by the end of the twenty-first century in the eastern Himalaya. This shift will cause the endemic flora to lose at least ~20% of its current habitats, highlighting the necessity to reassess the effectiveness of current conservation networks and policies over the Himalaya.

At high elevations, the potential upper range limit for trees is set by low temperatures[1,2]. The treeline, the line that connects the uppermost, undisturbed group of trees of a certain height[3,4,5] is one definition of this potential upper range limit. The treeline is also recognized as the cold edge of the fundamental niche of trees[6]. In the real world, trees do not always fully realize their fundamental niches: locally or regionally, they may not reach their treeline elevation and instead remain confined to lower elevations. Compared to the high-elevation thermal treeline, which is understood as a global phenomenon and is determined by a common seasonal mean temperature[7,8], much less attention has been given to this upper range limit of the realized niche of trees, simplified hereafter as the realized range limit of trees. Detailed study of the realized range limit of trees could help to develop theories of tree distribution near the treeline[9–12] and enhance our capacity to accurately estimate the space of tree infilling near the treeline in a warmer climate, which has important implications for plant community reshuffling and biodiversity conservation[13,14]. However, such studies require spatially explicit mapping of the realized range limit of trees and improved quantitative modelling of the relationship between the realized range limit of trees and its local or regional drivers.

The Himalaya is the world's highest mountain range and also has the world's highest treeline[15]. It harbours an exceptionally rich endemic alpine flora[16–18]. Climate change is occurring rapidly in the Himalaya, with a warming rate higher than the global average[19]. Such rapid climate change could induce upslope tree expansion, which may disadvantage existing endemic flora[20]. Understanding such climate change-induced shift in the upper range limit of trees and its potential impacts on regional alpine flora, especially those endemic ones, is key to informing management and conservation measures for the unique Himalayan flora. Currently, however, information on the Himalayan realized range limit of trees is mostly restricted to local field surveys of limited spatial extent[21–23]. Many important questions remain unanswered. For example, considering the broad range and diverse climates of the Himalaya, does the Himalayan realized range limit of trees follow the treeline position initially proposed in the time of Alexander von Humboldt[3]? If not, what are the important processes causing the deviation of the realized range limit of trees from the treeline? Addressing these questions could shed light on recent reports that historical shifts in the Himalayan upper range limit of trees are not always synchronous with warming[24,25,26]. More importantly, regional spatially explicit assessments of the Himalayan realized range limit of trees, including the modelling of its climatic dependence, are needed for predicting possible shifts in the realized range limit of trees and associated changes in the suitable habitat area for Himalayan endemic flora in a changing climate.

Results and discussion

A map of the Himalayan realized upper range limit of trees. Here, we used satellite-derived percentage tree canopy cover data at a spatial resolution of 30 m produced by the University of Maryland Global Land Analysis & Discovery laboratory (v.1.8; ref. [27]), to map the realized range limit of trees over the Himalaya circa 2015

[1]State Key Laboratory of Tibetan Plateau Earth System and Resources Environment (TPESRE), Institute of Tibetan Plateau Research, Chinese Academy of Sciences, Beijing, China. [2]School of Life Sciences, Lanzhou University, Lanzhou, China. [3]Key Laboratory for Earth Surface Processes of the Ministry of Education, Institute of Ecology, College of Urban and Environmental Sciences, Peking University, Beijing, China. [4]CAS Key Laboratory of Tropical Forest Ecology, Xishuangbanna Tropical Botanical Garden, Chinese Academy of Sciences, Mengla, China. [5]Department of Biology and Graduate Degree Program in Ecology, Colorado State University, Fort Collins, CO, USA. [6]Sino-French Institute for Earth System Science, College of Urban and Environmental Sciences, Peking University, Beijing, China. ✉e-mail: twang@itpcas.ac.cn

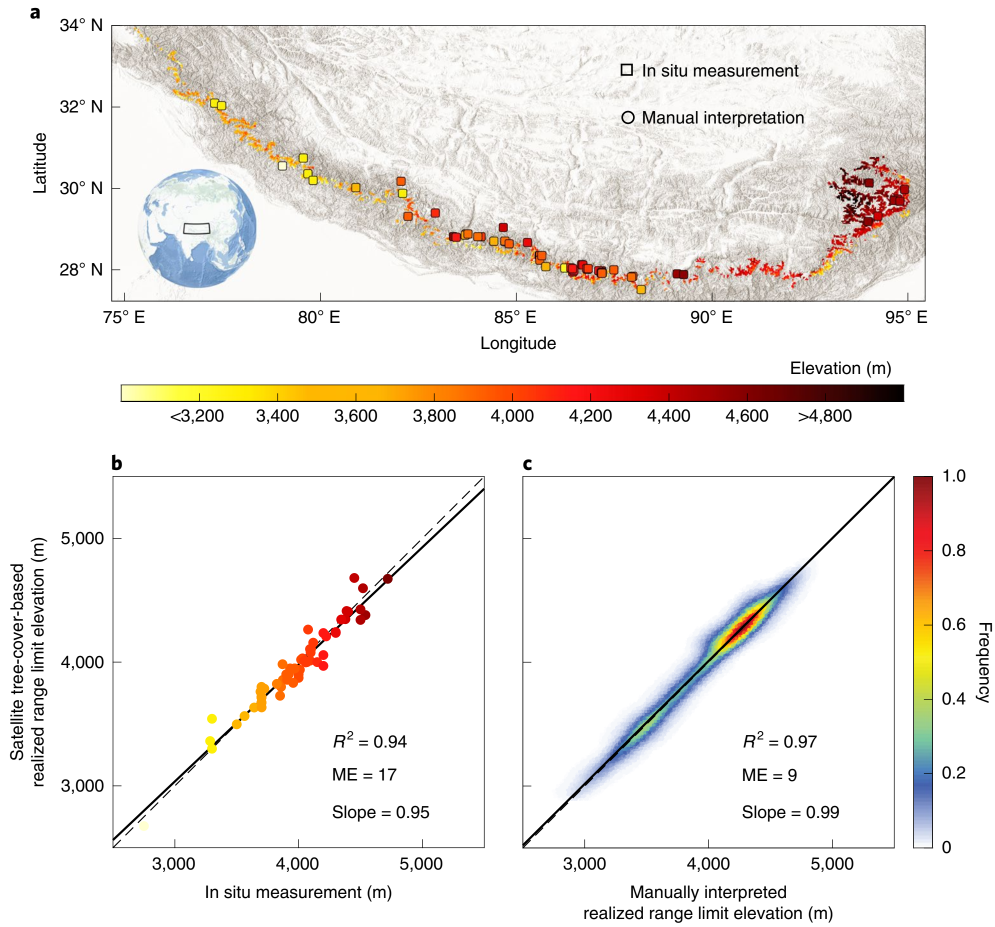

Fig. 1 | Calibration and validation of satellite tree-cover-based realized range limit of trees across the Himalaya. a, The spatial distribution of in situ measured upper range limit of trees (rectangles with border, $n=63$) and manually interpreted realized range limit of trees from Google Earth high-resolution images ($n=738{,}402$ at 30 m resolution) across the Himalaya. **b**,**c**, The relationships of satellite tree-cover-based realized range limit of trees with in situ measurements (**b**) and manual interpretation (**c**), with the 1:1 line (dashed) and the regression line (continuous). The satellite tree-cover-based realized range limit of trees is obtained using a tree-cover threshold of 10%, which is optimized on the basis of 63 in situ measurements. R^2 and ME indicate the coefficient of determination and the mean error, respectively.

(Methods). For this purpose, we developed an automatic algorithm that can produce a consistent characterization of realized range limit of trees across space. Using 10% tree cover as the threshold, we first delineated forested areas from the percentage tree-cover data and generated a forest boundary map from which to extract the realized range limit of trees. We then developed an elevational threshold approach to eliminate any possible interference of the lower forest boundary in the process of identifying the realized range limit of trees at the Landsat pixel scale (Methods). We used 63 in situ observations of upper range limit of trees across the Himalaya (Supplementary Table 1), to calibrate the tree-cover threshold used to delineate the forest boundary. The 10% tree-cover threshold was selected since the extracted realized range limit of trees determined using this value had the highest correlation ($R^2=0.94$, slope = 0.95, mean error (ME) = 17 m) with the in situ observations (Fig. 1a,b).

To validate the robustness of the satellite tree-cover-based elevational distribution of the realized range limit of trees, we built an independent validation dataset by manually interpreting the realized range limit of trees using Google Earth's high-resolution images (Methods). We produced 738,402 manually interpreted validation samples at a spatial resolution of 30 m over the Himalaya (Methods), with 146,604 (19%), 152,602 (21%) and 439,196 (60%) located in western, central and eastern Himalaya, respectively (Fig. 1a). Across all samples, the satellite tree-cover-based realized range limit of trees showed good agreement with the manually interpreted data at 30 m resolution ($R^2=0.97$, slope = 0.99, ME = 9 m) (Fig. 1c). For example, the first (2,956 m) and 99th percentiles (4,708 m) of the manually interpreted realized range limit of trees were comparable to those (2,949 and 4,665 m) derived from the satellite tree-cover data for the Himalaya. High levels of agreement between the satellite tree-cover-based and manually interpreted values of realized range limit of trees were also found if the western ($R^2=0.99$, slope = 0.98, ME = 15 m), central ($R^2=0.99$, slope = 0.99, ME = 14 m) and eastern regions ($R^2=0.98$, slope = 0.97, ME = 12 m) were considered separately (Extended Data Fig. 1). Since our satellite tree-cover-based data analysis is spatially explicit and consistent and therefore permits comparisons across very wide areas, it closes the knowledge gap on the spatial pattern of realized range limit of trees over the Himalaya.

The realized range limit of trees at a 1 km spatial resolution (Fig. 2) was produced from the original 30 m grid by calculating the mean value in each 1 km grid cell (Methods). The map shows that there is a great spatial variation in realized range limit of trees, with the lowest (first percentile) and highest (99th percentile) values being 2,933 and 4,639 m, respectively, and the mean standard deviation reaching 475 m. The realized range limit of trees increased along a longitudinal gradient, with relatively low values in western (3,370 ± 222 m) and central Himalaya (3,466 ± 310 m) and high ones

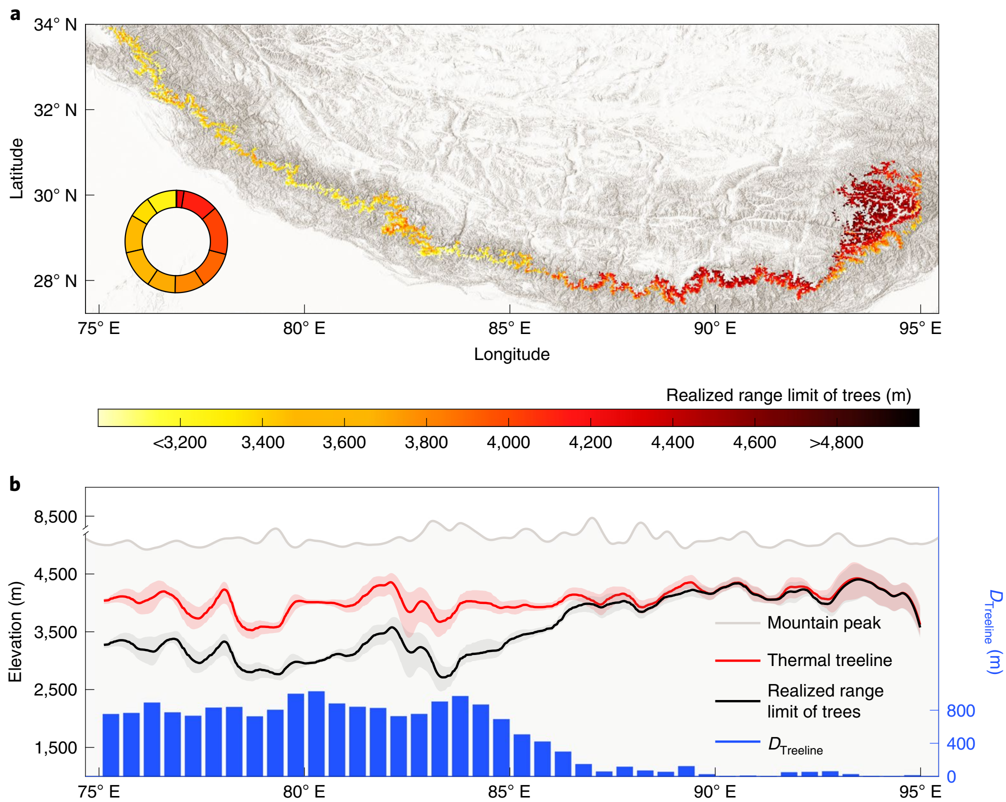

Fig. 2 | Elevational distribution of the realized range limit of trees across the Himalaya. **a**, Spatial distribution of realized range limit of trees at 1km resolution. The insets show the frequency distribution of realized range limit of trees. **b**, Changes of the mountain peak elevation, treeline elevation, satellite tree-cover-based realized range limit of trees and the deviation (D_{Treeline}) of realized range limit of trees from treeline elevation along the longitudinal gradient. Solid lines indicate the median value of each elevational category with longitude at a 1km interval, with the curve smoothed using the Loess function and the coloured shading representing 1s.d. Bars are the median values of D_{Treeline} with longitude, at 0.5° intervals.

in eastern Himalaya (4,167 ± 282 m). This large variation occurs within a very narrow latitudinal range (~7°), which is similar to the latitudinal variation of treeline elevation observed in the Northern Hemisphere between 70° and 45° N (ref. [7]).

Drivers of spatial variation in realized upper range limit of trees. We compared satellite tree-cover-based realized range limit of trees to the treeline elevation that is physiologically controlled by low temperature[7]. The mean growing-season temperature is often used as a robust estimation of the thermal treeline elevation that is exempt from human land use or other disturbances[8]. Analysis of a collection of in situ elevation measurements between 68° N and 42° S indicates that the mean growing-season ground temperature at a soil depth of 10 cm at the thermal treeline elevation shows little variation across the globe and is generally 6.7 ± 0.8 °C (ref. [7]). This ground temperature corresponds to a mean growing-season air temperature at 2 m above the ground (T_{air}) of 6.4 ± 0.7 °C and a mean growing-season land surface skin temperature (T_{skin}, the radiative temperature of the land derived from the thermal infrared radiation emitted by the surface[28]) of 7.6 ± 1.0 °C (Supplementary Table 2 and Extended Data Fig. 2). The values of these two types of temperature threshold are inferred from a strong across-site relationship between ground temperature and collocated T_{air} from WorldClim[29] or T_{skin} from the Moderate Resolution Imaging Spectroradiometer (MODIS), across more than 30 locations worldwide (Extended Data Fig. 2b,c). Using these two temperature thresholds, the average value of thermal treeline elevation (4,058 ± 335 m) across the Himalaya is ~400 m higher than the realized range limit of trees (3,633 ± 475 m).

We further examined the longitudinal pattern of the deviation of the realized range limit of trees from treeline elevation (D_{Treeline}) (Fig. 2b). D_{Treeline} has a sharp contrast from west to east, with values in western Himalaya of 761 ± 182 m compared with 35 ± 90 m in eastern Himalaya (Extended Data Fig. 3). For the eastern Himalaya, >80% of the realized range limit of trees have an associated mean growing-season T_{skin} that falls within the range of 7.6 ± 1.0 °C or mean growing-season T_{air} in the range 6.4 ± 0.7 °C and therefore reach the thermal treeline position. On the contrary, in the central and western Himalaya, only 12.1% and 1.0%, respectively, of the realized range limit of trees reach the thermal treeline position. To try to understand why D_{Treeline} has this sharp contrast along the longitude gradient, with large values in western and central Himalaya but small ones in the eastern Himalaya, we investigated the factors and processes that can cause trees to be absent from treeline positions.

The factors contributing to the deviation of trees from the treeline position can be contextualized into the major categories of climatic limitation, disturbances (including anthropogenic activities and earthquakes), soils and topography (Supplementary Table 3; Methods). We used a random-forest algorithm[30] to rank the importance and influence of the available variables from different categories on D_{Treeline} across the Himalaya (Fig. 3; Methods). Our analysis showed that a small number of variables, including premonsoon (March to May) cumulative climatic water deficit (CWD), anthropogenic disturbance (ANT) and premonsoon vapour pressure deficit (VPD) could predict nearly 80% of the spatial distribution in D_{Treeline}. Other factors, including topography and soils, explained only ~10% of the spatial variation in D_{Treeline}.

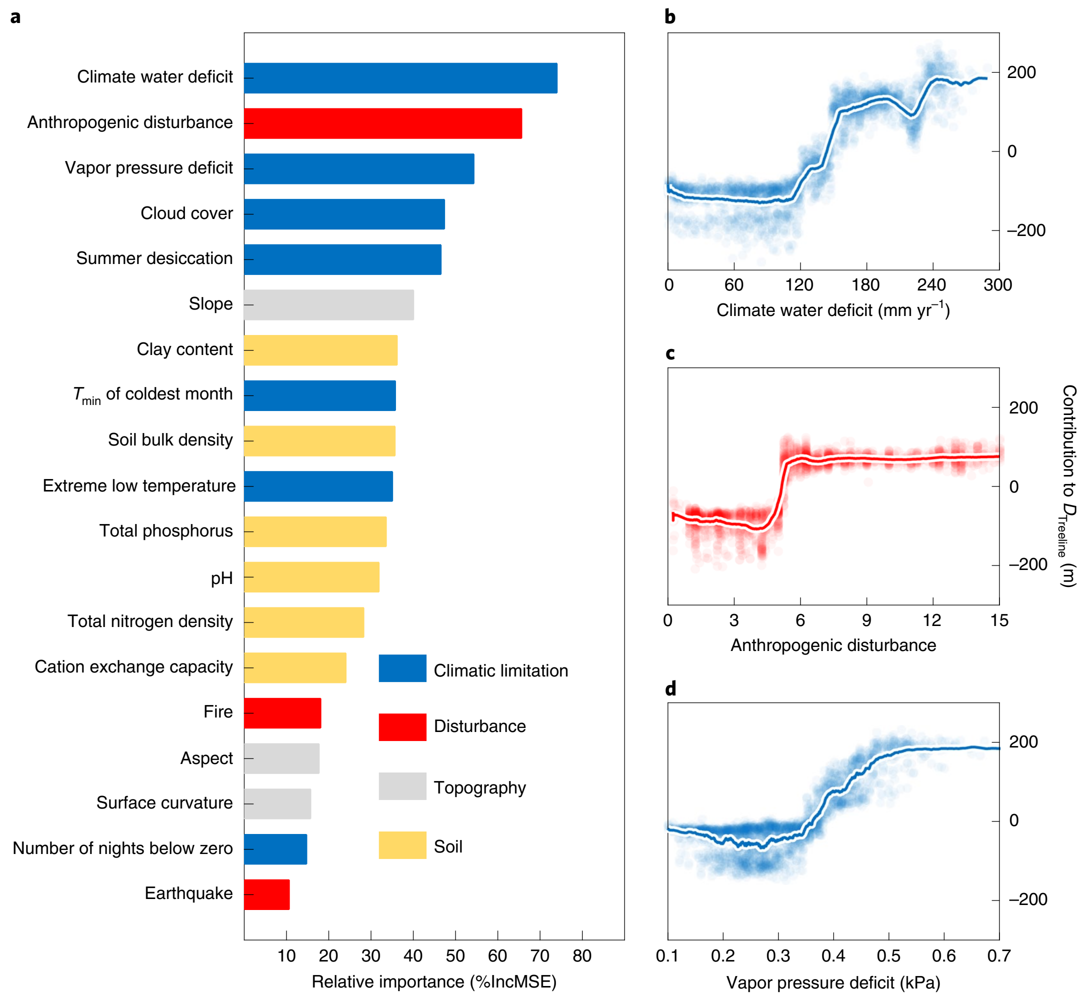

Fig. 3 | Variables predicting spatial pattern of D_{Treeline}. **a**, Relative importance of different categorical variables in predicting the spatial variation of D_{Treeline}. %IncMSE is the percentage increase in mean squared error. **b–d**, Partial contribution of the three most important variables to the spatial pattern of D_{Treeline}: premonsoon CWD (**b**), ANT (**c**) and premonsoon VPD (**d**). D_{Treeline} is the deviation of realized range limit of trees from treeline elevation. The partial contribution plot shows the impact of a certain independent variable (shown in the *x* axis) on D_{Treeline} for each grid (coloured point) while controlling for the impacts of changes in all other variables. For better visualization, we also plot the fitted line (coloured line) for each grid using leave-one-out *k*-nearest neighbour.

We then assessed how spatial changes of the leading factors (CWD, ANT and VPD) modulated the regional distribution of D_{Treeline}, with its sharp contrast between eastern and central western Himalaya (Fig. 2b). First, the abrupt D_{Treeline} transition occurring at the CWD threshold of ~120 mm yr^{-1} separated the eastern Himalaya, with the low CWD and D_{Treeline} values, from central to western Himalaya with the high ones (Fig. 3b and Supplementary Fig. 1a). The transition of D_{Treeline} along the VPD gradient further sharpens the observed west–east contrast, with western Himalaya having higher VPD than the eastern Himalaya (Supplementary Fig. 1b). Second, there is an anthropogenically driven D_{Treeline} gradient, with an abrupt transition occurring at the threshold of 5 (unitless) along the ANT gradient[31] (Fig. 3c). It separates central Himalaya (Bhutan) and the eastern Himalaya, which both have relatively low levels of human intervention (3.7 ± 3.1) and relatively low D_{Treeline} (30 ± 40 m), from the other regions that have intense human activity (8.5 ± 3.7) and relatively high D_{Treeline} (652 ± 301 m) (Supplementary Fig. 1c). Using thresholds for these two leading factors (CWD and ANT), we classified the pixels in locations where trees are absent from the treeline position into drought-, anthropogenic- or both-driven categories. We found that >73% of the pixels were in the category that is driven by both drought and ANT. Around 15% of the pixels, most of which are located in western Himalaya, belong to the drought-driven category. Only 6% of the pixels, scattered in the central Himalaya, belong to the anthropogenic-driven category. These results highlight the critical role of the premonsoon drought and ANT in shaping the west-to-east contrast in D_{Treeline}.

The drought-induced absence of trees from the treeline position can be attributed to the fact that moisture limitation, when it exceeds a certain threshold, can prevent the successful recruitment of tree seedlings. For example, dendrochronological studies in the central Himalaya, have shown that when premonsoon moisture levels fall below a critical minimum threshold, tree seedling establishment is prevented, thereby restricting the shift of the upper range limit of trees to higher elevations[32]. In addition, according to our interpretation of high-resolution images from Google Earth (Supplementary Fig. 2), trees can also reach the high-elevation treeline position in extrazonal habitats which locally deviate from the average dry conditions in the arid western Himalaya. The existence of such extrazonal habitats can be attributed to the alleviation of moisture limitation due to the proximity of ravines with moister conditions at high elevations[33]. This is the case with *Myricaria elegans*

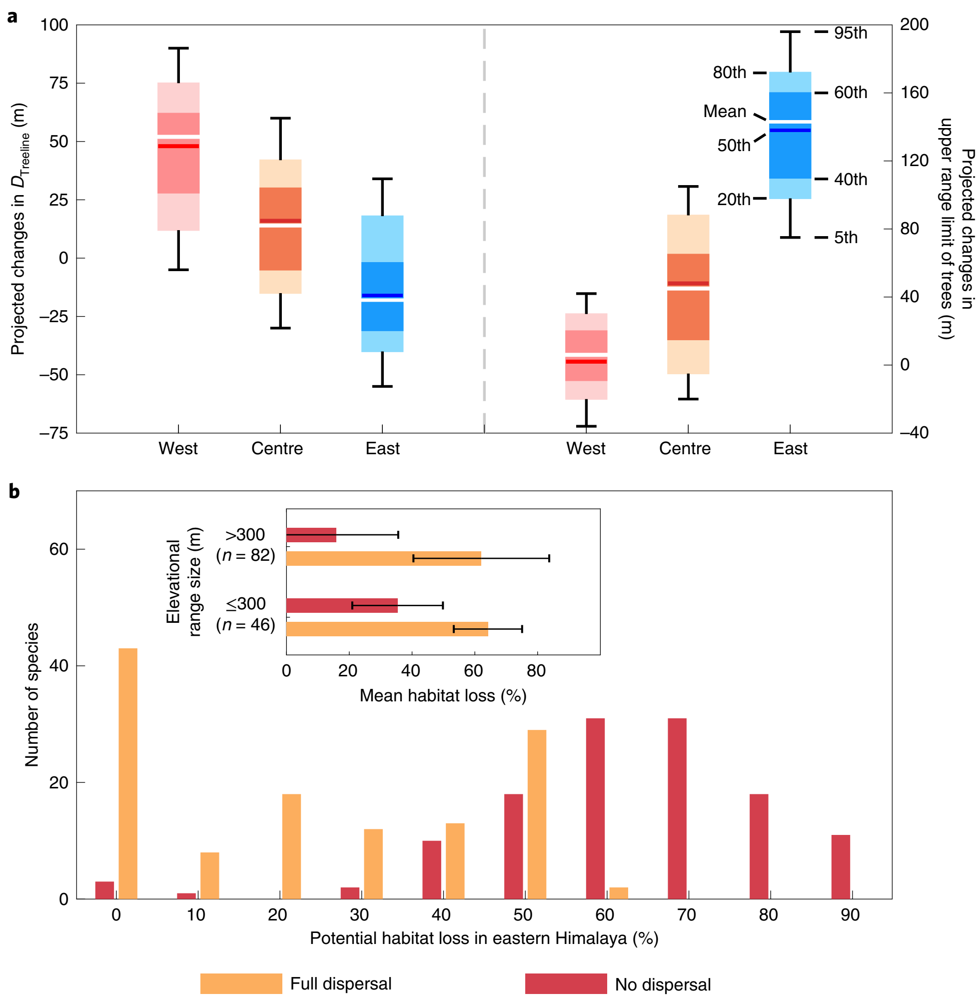

Fig. 4 | Projections of the upslope shift of upper range limit of trees and its impact on the habitat loss of the endemic flora at the end of this century. **a**, Projected changes in $D_{Treeline}$ (left) and upper range limit of trees (right) between periods 2080–2099 and 1995–2014 for western, central and eastern Himalaya, respectively, using CMIP6 multimodel ensemble mean under the SSP2-4.5 scenario. The whiskers and boxes represent the 5th, 20th, 40th, median, 60th, 80th and 95th percentiles and the white lines show mean values. **b**, Frequency distribution of upslope tree expansion induced habitat loss for alpine endemic flora in eastern Himalaya under the full and no dispersal scenarios. The inset panel shows the mean habitat area loss across two elevational ranges (≤300 m, with $n = 46$ and >300 m, with $n = 82$), with error bar representing 1 s.d. $D_{Treeline}$ is the deviation of realized range limit of trees from treeline elevation.

growing near glacial-fed streams in the northern Ladakh[34] for example. The anthropogenic activities can also be observed to be playing a role in slowing the historical upslope shift of the upper range limit of trees. For example, we assembled data from >30 sites across the Himalaya and its surrounding region where the upper range limit of trees was reconstructed using dendrochronological methods (Supplementary Methods 1) and changes in the upper range limit of trees were reported as either no change or advance (Supplementary Table 4). Our analysis shows that the advance rate in the past century declined with increasing human disturbance (Supplementary Fig. 3). Therefore, the identification of these factors in explaining the spatial pattern of $D_{Treeline}$ also provides mechanisms for understanding a divergent change in upper range limit of trees over the Himalaya, where, for example, most of the trees at the upper range limit over western Himalaya have remained stable, while they have experienced significant upslope shifts over eastern Himalaya[25,32].

Projections of the upper range limit of trees and its impact. The existence of an abrupt $D_{Treeline}$ transition along the climatic gradient (Fig. 3) indicates that the realized range limit of trees at locations near the threshold is particularly vulnerable to changing its elevation as climate changes. To illustrate the response of $D_{Treeline}$ to future climate change by the end of this century, we used the climate–$D_{Treeline}$ model derived from contemporary spatial patterns to infer future changes in $D_{Treeline}$ (Methods). This spatial model encompassed spatial climatic gradients similar to the temporal ones expected by the end of this century, giving us a relatively high level of confidence in the projections (Supplementary Figs. 4 and 5). Using Coupled Model Intercomparison Project Phase 6 (CMIP6) multimodel ensemble mean projection (Supplementary Table 5) to apply the established model to the end of this century (2080–2099), we found that, under Shared Socioeconomic Pathways (SSP)2–4.5, changes in $D_{Treeline}$ will increase in western (52 ± 21 m) and central Himalaya (16 ± 14 m) and decrease in the eastern Himalaya (-18 ± 17 m) (left panel of Fig. 4a). This spatial divergence in $D_{Treeline}$ change is projected because the increase will predominantly occur in regions that become drier, with the decline occurring in regions that become wetter (Supplementary Fig. 6). In western and central Himalaya, the future aggravation of drought will impede the capacity of trees to track the treeline position. In contrast, in eastern Himalaya where drought does not occur at the upper range limit and the climate will further become wetter in the future, the upper trees would then be able to track the treeline position. Since the treeline position will shift upwards in a warming world, the upper range limit of trees will shift upwards to a much greater extent in eastern Himalaya (143 ± 43 m) than in central (45 ± 39 m) and western Himalaya (6 ± 14 m) (right panel of Fig. 4a). Note that our projection of future changes in D_{Treeline} represents the potential impact of climate change without considering human activities. If anthropogenic disturbance persists or intensifies in the western and central Himalaya, the projected increase in D_{Treeline} would be further enlarged, possibly even resulting in a decline in the upper range limit of trees in a warmer world.

To quantify upshift-induced potential habitat loss for high-elevation endemic flora in eastern Himalaya[35], we collated 128 endemic species belonging to 49 genus and 24 families (Supplementary Table 6), which have been reported above the upper range limit of trees (Methods and ref. [36]). For each of these endemic species, the potential habitats for current and future periods were the sum of the surface area of pixels at a spatial resolution of 30 m, whose elevations were above the realized range limit of trees and within the species elevational range. The habitat loss is then calculated as the percentage difference between the areas of current and future habitats (Methods). We assumed two species dispersal scenarios: for the 'no dispersal' scenario, species would not migrate; while for the 'full dispersal' scenario, endemic species would migrate upslope by the same distance as the upper range limit of trees did. Our results show that the potential habitat, averaged across all endemic species, will shrink by 23 ± 20% under the full dispersal scenario, since the surface area would shrink with increased elevation and new upslope habitats could not compensate for this loss[14]. The habitat loss would increase to 63 ± 18% under the no dispersal scenario (Fig. 4b). Moreover, this shift will lead to a disproportionate loss of potential habitats, with species with only a narrow range of elevations (≤300 m), suffering losses of 35 ± 21% and 64 ± 10% under full and no dispersal scenarios, respectively, while those with a wide range of elevation (>300 m) will suffer losses of 15 ± 16% and 62 ± 14% for the same scenario, respectively (Fig. 4b). This result highlights that, under future climate change, habitat loss will be aggravated for local endemic species with a narrower range.

Conclusion

We used high-resolution, remotely sensed data to provide a spatially consistent and ground truth-validated map of the realized range limit of trees across the Himalaya. We show that drought and anthropogenic activities are the primary factors that cause trees to be absent from the thermal treeline position set by the seasonal mean temperature, thus contributing to the low realized range limit of trees in central and western Himalaya and the high one in the eastern Himalaya. The identification of these factors offers significant insights into the mechanisms behind the stable upper range limit of trees as they are widely reported for the central Himalaya. One clear implication is that using changes in the upper range limit of trees as a source to document past climatic warming, especially in the central and western Himalaya, would be ineffective and should only be done with great caution. Trees in eastern Himalaya could closely track a warming-induced upward shift of treeline position and such an upslope tree expansion in a warming world will lead to habitat loss for the alpine endemic flora in this region, especially where the alpine belt is very narrow. Our findings provide baseline information for policy-makers and stakeholders, as well as for initiatives that aim to protect endemic species of high conservation value. They also highlight the necessity to reassess the effectiveness of current conservation networks and policies over the Himalaya. Open migration corridors and retention of connections between regions with a narrow alpine belt (low elevation mountains) and regions with a wide alpine belt (very high mountains) will become very important in a warming world[4,37].

Methods

Mapping the realized range limit of trees. We aimed to determine the upper range limit of the life-form tree, which we consider here to be the upper boundary of tree distribution. For this purpose, we used percentage tree canopy cover data[27] at a spatial resolution of 30 m to delineate forested areas, with the resulting map forming an input for forest boundary (edge) extraction (Supplementary Fig. 7). We used percentage tree-cover data for the year 2000 and annual tree-cover loss and gain data (https://earthenginepartners.appspot.com/science-2013-global-forest), which are produced by the University of Maryland Global Land Analysis & Discovery laboratory (v.1.8; ref. [27]), to obtain the percentage tree-cover data circa 2015. These data were derived from Landsat 7 Enhanced Thematic Mapper Plus (ETM+) and Landsat 8 Operational Land Image (OLI) (for 2013 onward) scenes, with the reflectance of Landsat time-series images calibrated and normalized using MODIS reflectance datasets[38]. Note that the tree-cover gain data were not updated after 2012. The tree-cover data circa 2015 were obtained by aggregating the percentage tree cover for the year 2000 with the tree cover loss between 2000 and 2015 and the gain between 2000 and 2012.

Preprocessing satellite tree-cover data. To calibrate the threshold of tree-cover fraction for the determination of forested areas, we first compiled a list of in situ measured upper range limit of trees made over the Himalaya (Fig. 1a). Although making in situ observations is time-consuming and labour-intensive in remote Himalayan regions, and therefore they are relatively rare, we were able to gather 108 samples by reviewing the prior literature. Following sampling strategies described elsewhere[39], we only considered data representing the upper range limit of trees with upright stems and we excluded samples that recorded the position of single trees, seedings or krummholz. We also excluded samples if the precision of their latitude/longitude coordinates was worse than 1 km or if the area had been disturbed by fire or human activities. Any in situ positions reported for the period before 1985 were also excluded because of possible movement in response to historical environmental change. This filtering resulted in 63 observations being available for calibration (Supplementary Table 1). The tree-cover threshold used to define forested area was optimized as 10% (Fig. 1b) which is consistent with the value used by the Food and Agriculture Organization[40].

Using these in situ measurements to calibrate our more recent satellite-derived observations (circa 2015) would be problematic if trees over the Himalaya had a large upward shift in the past three decades. To investigate this potential bias, we compiled in situ historical dynamics in the upper range limit of trees, which were reconstructed using the dendrochronology method (Supplementary Methods 1), to show that the upper range limit of trees across the Himalaya advances from 0 to 80 m across varying time periods (71–193 yr), with a mean estimate of 1.4 ± 1.7 m per decade (Supplementary Table 4). A rough estimate is that the upper range limit of trees would have shifted upwards by ~4 m in the past three decades. This magnitude of shift is well within the calibration uncertainties of the upper range limit of trees (~17 m in elevation). The overall uncertainty in calibrating the upper range limit of trees, measured as the mean error between in situ observation and satellite tree-cover-based realized range limit of trees, was 17 m. On the basis of this calibrated tree-cover threshold, we transformed the satellite percentage tree-cover data into a binary image in which forest pixels have a value of 1 and non-forest pixels have a value of 0. The identification of the upper forest boundary from this derived forest map could be confounded by small non-forest patches ('inner non-forest patches') (Supplementary Fig. 8a) or small forested strips that are discrete from a contiguous forested area ('outpost-forest patches') (Supplementary Fig. 8b). To avoid these problems, we filled 'inner non-forest patches' using a widely used hole-filling technique[41] which eliminates internal voids and keeps the forest boundaries unchanged and also removed 'outpost-forest patches' with an area <0.5 ha. In addition, we ignored permanent snow-cover pixels using the MODIS snow-cover product (MOD10A1).

Generating the regional forest boundary elevation dataset. The processed forest map was used as the input for forest boundary extraction, an edge-detection process, which aims to find the discontinuities or abrupt changes in the image. We adopted the Canny edge detector, an efficient multistage edge-detection algorithm, to detect a wide range of edges in the forest image[42]. In the first stage, we smoothed the forest image with a Gaussian filter and removed any unwanted pixels that did not constitute forest edges by finding the local maxima in intensity gradients. In the second stage, an intensity gradient threshold must be defined to determine which of the remaining edge pixels are real edges. The ranges for the size of the Gaussian filter and the threshold of the intensity gradients are 1–5 and 10–50, respectively. We randomly selected ~10,000 manually interpreted upper range limit of trees from southeastern Tibet to find the optimal values for the size of the Gaussian filter and the threshold value, which were 3 and 30, respectively. The process of setting these two parameters does not require intensive trial-and-error and using different parameter values was shown to have a marginal effect on the elevation of delineated upper edges. To ensure independent sample validation, those manually interpreted data used for calibration of the Canny edge detector were removed in the validation section. We then extracted the elevation of the forest edges from the digital elevation model (DEM) dataset provided by the Shuttle Radar Topography Mission at 30 m resolution.

Delineating the realized range limit of trees. The resultant forest-edge image contains both the lower and upper forest edges. To obtain just the upper edges that we require, we removed the lower forest boundary by defining a threshold of elevation below which edge pixels were removed. The application of a single universal elevational threshold over the Himalaya, which has a huge altitude range and complex topography, would be problematic, so we developed a local adaptive algorithm that calculated the threshold by iterating over a range of window sizes until no more edge pixels are removed (Supplementary Fig. 7).

The first step in this process is to construct a histogram of forest-edge elevation within a window size of w centred on a geographical point of the 0.1° mesh of the forest-edge image. The ranges of the minimum and maximum window size were empirically set as 0.01–0.5° and 0.5–1°, respectively, using the criterion that the window should not be too small to include either upper or lower edges but should also not be so large as to include some lower edge pixels having even higher elevations than the upper-edge pixels. On the basis of trial-and-error, we set the minimum and maximum window sizes to 0.1° and 1°, respectively. We tested the robustness of the elevation of the delineated upper edge to the use of different minimum and maximum window sizes and found that different combinations yielded similar elevations as our trial-and-error combination (0.1° and 1°). However, the trial-and-error combination is among the fastest ones to identify the value of w, taking half the time of the slowest combination. We initialized w with 1° and started an iterative process with a w decrement of 0.1° until a stopping criterion was satisfied. The second step is to test the unimodality of the distribution within a given window size. We smoothed the histogram using a Savitzky–Golay filter of 3° and assumed that the smoothed distribution was the integration of one or more Gaussian functions. The unimodality of the distribution could then be tested by determining the number of Gaussian functions (n) in the data. The third step is to model the distribution of the histogram if n was larger than 1. We modelled the data distribution for this case with n Gaussian functions using the trust region reflective algorithm[43].

$$y = \sum_{i=1}^{n} a_i e^{\left[-\left(\frac{x-\mu_i}{\sigma_i}\right)^2\right]} \quad (1)$$

where a_i, μ_i and σ_i are amplitude, centroid and standard deviation for i of n respectively. We defined the threshold of elevation below which edge pixels within the given window are removed as:

$$\left\{ \begin{array}{l} \text{If } a_{n-1} > a_n, \text{ Threshold} = \mu_{n-1} + 3\sigma_{n-1} \\ \text{If } a_{n-1} < a_n, \text{ Threshold} = \mu_n - 3\sigma_n \end{array} \right\} \quad (2)$$

Using a w decrement of 0.1°, we iterated through the above three steps until n was equal to 1. When $n=1$, we moved to another geographical point of the 0.1° mesh and repeated the iterative process.

To assess the performance of this algorithm, we selected three regions and distinguished the upper edges from lower ones by manual interpretation based on high-resolution images from Google Earth (see the following section on validation). The validation showed that our local adaptive algorithm could successfully separate the lower forest edges from the upper ones in the three selected typical regions. The false upper-edge-detection rate was <5% and <6% of upper edges went undetected. Details of the added value of each processing steps are given in Supplementary Methods 2 and Supplementary Fig. 9.

Validating tree-cover-based realized range limit of trees. We validated the satellite tree-cover-based realized range limit of trees using manually interpreted values from high-resolution (HR) (<5 m) satellite imagery available on the Google Earth platform. This platform provides free access to preprocessed HR images that mainly originate from Digital Globe libraries and are acquired from various sensors with a spatial resolution of <5 m. The HR images are georeferenced with geolocation accuracies better than 10.8 m and were predominantly (85%) acquired after 2017. These characteristics make the use of such HR images to validate satellite tree-cover-based realized range limit of trees defensible. Here, we generated validation samples of upper range limits of trees at a spatial resolution of 30 m from the HR images across the Himalaya (Fig. 1a) as follows. We first counted the number of mountains, based on a mountain summit dataset[44]. For each mountain, we delineated the upper range limit of trees using the tones and texture information in the HR images. Compared to non-tree images, forest images are dark green with a rough texture with obvious crown shadows. We also resorted to field-based photographs obtained from Google Earth to assist with the interpretation. Discrimination between forest and non-forest images is therefore straightforward. To ensure a uniform quality of interpretation, we cross-validated the obtained samples using different interpreters and then had a single quality controller check all the results. We then rasterized the delineated realized range limit of trees to a spatial resolution of 30 m. According to the mountain summit dataset[44], there are 276 (17%), 339 (21%) and 1,003 (62%) mountain peaks in western, central and eastern Himalaya, respectively. For each mountain peak, we obtained ~500 validation samples at a spatial resolution of 30 m from the HR images on the basis of the procedures described above. We were able to obtain the total size of validation samples commensurate with the number of mountain peaks in western (146,604), central (152,602) and eastern Himalaya (439,196), respectively (Extended Data Fig. 1). Our analysis shows that satellite tree-cover-derived realized range limit of trees had a high level of consistency with the manually interpreted values derived from Google Earth images ($R^2=0.97$, slope = 0.99, ME = 9 m; Fig. 1c).

Calculating the treeline elevation. The treeline elevation is the physiological limit set by temperature and is the cold edge of the fundamental niche of trees[6]. The elevation of such a presumed thermal treeline is generally higher than the realized range limit due to the presence of anthropogenic influence, mechanical prevention (for example, rocks) and climatic stresses such as moisture shortage. Other studies[7] made continuous ground-temperature measurements at 46 treeline sites between 68° N and 42° S for the period 1996–2003 (Extended Data Fig. 2a and Supplementary Table 2). After disregarding taxon-, human- or fire-controlled upper limits, the thermal treeline was found to occur at a mean growing-season ground temperature of 6.7 °C at 10 cm depth ($n=30$). This temperature showed little variation, with a narrow amplitude of 2.2 °C for different climate zones[7]. It is important to note that there can be discrepancies between the position of trees that was established during different periods and the period for which the applied climatic data have been obtained.

To determine the Himalayan thermal treeline position, we used two different temperature datasets: the land surface skin temperature (T_{skin}) and the air temperature (T_{air}). Initially, we used the daily T_{skin} dataset from Collection 6 of MODIS at a spatial resolution of 1 km. This remotely sensed T_{skin} gives reliable and true coverage, in contrast to T_{air} which typically relies on a sparse network of meteorological stations in mountainous regions. First, we selected daily T_{skin} data, without cloud contamination, centred on each treeline site reported in ref. [7] during the period 2002 to 2018. However, there is only one year of overlap between the MODIS T_{skin} (2002–2018) and ground temperature at a soil depth of 10 cm (1996–2003) data at the treeline locations listed in ref. [7]. If not corrected for, this time mismatch between the datasets would lead to an inaccurate estimation of the growing-season temperature threshold for mapping treeline position and so the MODIS T_{skin} data for 2002–2018 must be corrected to 1996–2003 levels. Since long-term MODIS T_{skin} data dating back to 1996 do not exist, we estimated the change of growing-season skin temperature between 1996–2003 and 2002–2018 using the European Centre for Medium-Range Weather Forecasts Reanalysis v.5 (ERA5)[45] at each location (Supplementary Table 2). We assumed that the change in MODIS T_{skin} between these two periods is equivalent to that in the ERA5 skin temperature at each location, given that the skin temperature has a similar physical meaning as MODIS T_{skin} (ref. [46]). We then obtained the skin temperature values for 1996–2003 from those of 2002–2018 using the ERA5-derived temperature change between these two periods (Supplementary Fig. 10). These data were averaged to produce daily climatological values of T_{skin} at the site level. Second, a threshold-based approach was adopted to determine the start and end of the growing season from the daily climatological T_{skin} values. Previous work[7] used a ground-temperature threshold of 3.2 °C at 10 cm depth to define the start and end of the growing season. We then optimized the T_{skin} threshold to achieve the best fit with the ground-temperature-based start and end of the growing season over 30 climate treeline sites. Our analysis revealed that the best correspondence (least root mean-squares error and highest coefficient of determination) occurred when the beginning of the season was defined as the date at which daily T_{skin} rises above 0.7 °C and the end of the season as the date at which it falls below 0.7 °C. Using this T_{skin} threshold, we calculated growing-season mean T_{skin} over the Himalayan region at a spatial resolution of 1 km. Third, we performed a regression analysis between growing-season mean T_{skin} and ground temperature at a 10 cm depth across all the treeline sites (Extended Data Fig. 2b) and found that the treeline occurred at the growing-season mean T_{skin} of 7.6 ± 1.0 °C (Supplementary Table 2). This growing-season mean T_{skin} was then used to map the Himalayan-scale treeline elevation. Due to the inherent uncertainties of climate datasets, we also determined the treeline position from the isolines of growing-season mean T_{air} of 6.4 ± 0.7 °C based on the WorldClim[8] (Extended Data Fig. 2c), with the growing season defined as the period between the day when the weekly mean air temperature rose above 0.9 °C and the day when it dropped below this value. To combine these two results and give a single measure of treeline position over the Himalaya, we first derived the elevation of the isotherm and the associated range from both T_{skin} (7.6 ± 1.0 °C) and T_{air} (6.4 ± 0.7 °C) and then calculated the treeline elevation by averaging the elevation derived from the two types of isotherms, with the uncertainty range defined by their highest and lowest values.

Thematic mapping of realized range limit of trees and $D_{Treeline}$. We mapped realized range limit of trees, treeline elevation and the deviation of realized range limit of trees from treeline elevation ($D_{Treeline}$) at a spatial resolution of 1 km. We first aggregated the realized range limit of trees from the original 30 m to 1 km resolution by calculating the mean value in each 1 km grid cell. $D_{Treeline}$ is set to 0 for pixels where the realized range limit of trees fell within the uncertainty range of the treeline elevation, indicating that the realized range limit of trees had reached the treeline position. There are uncertainties in the temperature datasets that might lead to the calculated treeline position being lower than the realized range limit of trees in some pixels. We therefore also set $D_{Treeline}$ to 0 for these pixels where the realized range limit of trees were well above the uncertainty range of the treeline elevation.

Variables explaining the spatial pattern of $D_{Treeline}$. *Assembling variables.* To identify the key drivers of the spatial pattern of $D_{Treeline}$, we assembled a broad set of variables on the basis of the availability of datasets: climate limitation (including premonsoon CWD[47,48], premonsoon VPD[49], cloud cover, minimum temperature (T_{min}) of the coldest month, the mean temperature of the coldest quarter, extreme low temperature in winter, the number of nights with temperature below freezing during the active growing period, summer desiccation[50] and winter frost risk[50]), disturbance (the number of fires[51], ANT[52–55] and magnitude of earthquake events[56]), soil (soil texture, bulk density, pH, cation exchange capacity, total phosphorus and total nitrogen density) and topography factors (slope gradient, surface curvature and aspect). For details about variables, please refer to Supplementary Methods 3 and Supplementary Table 3. Note that there are other variables that are not considered in our analysis[57–59] (Supplementary Methods 3).

Variable-importance analysis. Although collinearity among variables would not affect the predictive accuracy of the random forest, it does affect variable-importance ranking because variables with strong collinearity could cancel each other out[60], thereby affecting the interpretability of variables. To minimize the confounding effect of strong collinearity on variable importance, we detected multicollinearity using variance inflation factors within each category (climate limitation, disturbance, soil and topography)[61]. This procedure led to the mean temperature of the coldest quarter, winter frost and sand content being excluded, due to their high variance inflations (VIFs $\geq$ 3). We then used a random-forest approach to rank the relative importance of all predictor variables using all the $D_{Treeline}$ data at 1 km resolution. The random forest is a non-parametric modelling technique and capable of capturing nonlinearities and interactions among independent variables, without making any assumptions of the data[30]. A strength of the random forest is that we do not have to specify aspects such as the order of independent variables and their interactions and the random forest itself can discover inherent patterns and avoid overfitting effectively in a very large dataset. Random forest created an ensemble of decision trees, each of which is constructed using a different bootstrap sample from approximately two-thirds of the original data. The unused data are known as out-of-bag (OOB) observations. A regression for OOB observations is predicted from a decision tree and the errors for that decision tree are then estimated from these OOB predictions. To assess the relative importance of each predictor variable, we randomly permuted the data for a predictor and evaluated the decrease in prediction accuracy as measured by an increase in the mean-squares error between the observations and the OOB predictions. The importance of each variable is then computed from the average of the decrease over all decision trees (200 trees in this study). We then used the 'forestFloor' package in R statistical software (http://cran.r-project.org/) to visualize the partial contribution of $D_{Treeline}$ to the relatively important predictors (Fig. 3) and all the predictors (Supplementary Fig. 11). The partial response of $D_{Treeline}$ to an important predictor often forms a curve with a well-defined tipping point (clear maxima or minima) and the trees at locations near such a tipping point are vulnerable to changing their elevation as the predictor changes.

Projections of future climate change-induced $D_{Treeline}$. Both climate change and ANT could affect the shift of the upper range limit of trees in the future but ANT is difficult to predict because of its stochasticity. We therefore estimated $D_{Treeline}$ due only to climate change and used contemporary spatial patterns to construct a random-forest regression model (referenced to the climate–$D_{Treeline}$ model) from intact areas without significant anthropogenic activities. First, we approximated intact areas as the pixels with a human footprint index lower than 5, at which level ANT contributed little to explain the contemporary spatial pattern of $D_{Treeline}$ (Fig. 3c). Second, we used the recursive feature elimination method to filter variables used to construct a parsimonious climate–$D_{Treeline}$ model. As shown in Supplementary Fig. 12, the error declined steeply when using the most important five variables but it fluctuated and decreased only by <1% when using additional variables. We then constructed a climate–$D_{Treeline}$ model by including only five variables: premonsoon CWD, premonsoon VPD, cloud cover, summer desiccation and slope. This parsimonious model yielded a high performance (R^2 = 0.81, slope = 0.85, ME = 32 m; Supplementary Fig. 13) and is less prone to errors in model extrapolation, since the inclusion of fewer predictor variables should result in a lower probability of predictors falling outside the range of the training dataset[62].

We applied our parsimonious climate–$D_{Treeline}$ model to project changes in $D_{Treeline}$ at the end of the twenty-first century (mean over the period 2080–2099). We derived projected multimodel mean climate variables (CWD, VPD, summer desiccation, cloud cover and slope) from Earth system models forced by integrated scenarios of future climate and societal change (SSP2–4.5) in CMIP6 (Supplementary Table 5). SSP2–4.5 is a pathway where the future socioeconomic development adopts a middle-of-the-road scenario and the radiative forcing peaks at 4.5 W m^{-2} before the year 2100. We applied the delta approach to correct biases in future climate at a monthly timescale[63]. Besides, we also tested the robustness of this future $D_{Treeline}$ prediction, by quantifying the extent to which the five predictor variables (CWD, VPD, summer desiccation, cloud cover and slope) from the CMIP6 future projections fell within their historically observed ranges in the training data (Supplementary Methods 4). To map the shift in upper range limit of trees due to climate change at the end of the twenty-first century, we first estimated future treeline elevation using two temperature thresholds (T_{skin} of 7.6 ± 1.0 °C or T_{air} of 6.4 ± 0.7 °C) from temperature projections made under the SSP2–4.5 scenario and then calculated future upper range limit of trees as the difference between future treeline elevation and future $D_{Treeline}$ at a spatial resolution of 1 km. Note that changes in the upper range limit of trees would generally lag behind temperature changes because of factors such as the time needed to become established as a life-form tree, the presence of anthropogenic activities and environmental stresses (Supplementary Discussion).

Estimating potential habitat loss of the endemic flora. We obtained local distribution data for Chinese endemic species at the county level from published floras[64,65] and considered endemic species that are locally distributed in the eastern Himalaya and adjacent regions, where trees are projected to expand upslope dramatically. We then harmonized the names of species based on ref. [64] and selected the species, which are only found above the upper range limit of trees, on the basis of their elevational distribution, growth form and habitat, following ref. [36]. Specifically, the reported lower bound of elevational distribution for each chosen species had to be higher than the minimum upper range limit of trees at the county level. Moreover, the species habitat must not include forest, tree, river or road but must include at least one word from the following: cushion vegetation, meadow, grassland, scree, rock outcrop, snow bank or fell field. The application of these criteria resulted in a list of 128 alpine endemic species belonging to 49 genus and 24 families (Supplementary Table 6).

To estimate the current and future potential habitat for each endemic species, we first selected 1 km pixels, whose upper range limit of trees are lower than the upper bound of the species elevational range, across counties with occurrence records for the species under consideration. Second, within each 1 km pixel, we extracted the surface area of all 30 m subpixels using a 30 m resolution DEM and obtained a summed surface area from those 30 m subpixels that had elevations falling within the elevational range of the species in question. The suitable habitat for this endemic species was then estimated by summing up the surface area of all the selected 1 km pixels. The loss of potential habitat (as a percentage) induced by the upslope shift of the upper trees is then computed as the ratio of the difference between the current and future habitat to the current habitat.

To estimate future potential habitats (2080–2099), we considered two species dispersal scenarios: for the 'no dispersal' scenario, species would not migrate; for the 'full dispersal' scenario, endemic species would migrate upslope for the same distance as trees. Under the no dispersal scenario, the future habitat (2080–2099) is equal to the current one. Under the full dispersal scenario, we assumed that the endemic species could migrate to nearby habitats with higher elevations, especially those including the top of the mountain range, based on the criterion that these potential habitats fall within the species' elevational range and are physically connected with the current habitat. Specifically, we examine all surrounding 30 m resolution pixels within an area of 3 × 3 km^2 centred on the target pixel (current habitat) and, on the basis of a visual check, only select those pixels that are physically connected to the current habitat. The rationale for selecting surrounding pixels is that alpine endemic species generally live in microhabitats that are created by microtopography and thus decoupled from macroclimate conditions[66]. Microscale conditions are more important for these species' persistence than are macroclimate conditions[67,68]. Mountains, especially large ones, generally have a range of elevations and a relatively large areal extent, providing a rich diversity of microclimate conditions, even around the summit, with microrefugia providing suitable habitats for species persistence.

Reporting summary. Further information on research design is available in the Nature Research Reporting Summary linked to this article.

Data availability

All data needed to evaluate the conclusions in this paper are present in the paper and/or the Supplementary Information. The spatial distribution of manually interpreted and Landsat tree-cover-derived realized range limit of trees can be accessed through https://globalmapping.users.earthengine.app/view/realized-upper-range-limit-position-over-himalaya.

Code availability

All computer codes used in this study can be provided by the corresponding author upon reasonable request.

Received: 6 June 2021; Accepted: 22 April 2022;
Published online: 2 June 2022

References

1. Von Humboldt, A. *Cosmos: A Sketch of a Physical Description of the Universe* Vol. 5 (H.G. Bohn Press, 1895).

2. Körner, C. *Alpine Treelines: Functional Ecology of the Global High Elevation Tree Limits* (Springer, 2012).
3. Peñuelas, J., Ogaya, R., Boada, M. & Jump, A. S. Migration, invasion and decline: changes in recruitment and forest structure in a warming-linked shift of European beech forest in Catalonia (NE Spain). *Ecography* **30**, 829–837 (2007).
4. Körner, C. *Alpine Plant Life: Functional Plant Ecology of High Mountain Ecosystems* (Springer, 2021).
5. Körner, C. A re-assessment of high elevation treeline positions and their explanation. *Oecologia* **115**, 445–459 (1998).
6. Körner, C. The cold range limit of trees. *Trends Ecol. Evol.* **36**, 979–989 (2021).
7. Körner, C. & Paulsen, J. A world-wide study of high altitude treeline temperatures. *J. Biogeogr.* **31**, 713–732 (2004).
8. Paulsen, J. & Körner, C. A climate-based model to predict potential treeline position around the globe. *Alp. Bot.* **124**, 1–12 (2014).
9. Feeley, K. J. & Rehm, E. M. Downward shift of montane grasslands exemplifies the dual threat of human disturbances to cloud forest biodiversity. *Proc. Natl Acad. Sci. USA* **112**, E6084–E6084 (2015).
10. Lenoir, J. et al. A significant upward shift in plant species optimum elevation during the 20th century. *Science* **320**, 1768–1771 (2008).
11. Macias Fauria, M. & Johnson, E. A. Warming-induced upslope advance of subalpine forest is severely limited by geomorphic processes. *Proc. Natl Acad. Sci. USA* **110**, 8117–8122 (2013).
12. Morueta Holme, N. et al. Strong upslope shifts in Chimborazo's vegetation over two centuries since Humboldt. *Proc. Natl Acad. Sci. USA* **112**, 12741–12745 (2015).
13. Greenwood, S. & Jump, A. S. Consequences of treeline shifts for the diversity and function of high altitude ecosystems. *Arct. Antarct. Alp. Res.* **46**, 829–840 (2014).
14. Körner, C. & Hiltbrunner, E. Why is the alpine flora comparatively robust against climatic warming? *Diversity* **13**, 383 (2021).
15. Miehe, G. et al. Highest treeline in the northern hemisphere found in southern Tibet. *Mt. Res. Dev.* **27**, 169–173 (2007).
16. Myers, N. et al. Biodiversity hotspots for conservation priorities. *Nature* **403**, 853–858 (2000).
17. Wang, F. et al. Add Himalayas' Grand Canyon to China's first national parks. *Nature* **592**, 353–353 (2021).
18. Zhu, L. et al. Regional scalable priorities for national biodiversity and carbon conservation planning in Asia. *Sci. Adv.* **7**, eabe4261 (2021).
19. Yao, T. et al. Different glacier status with atmospheric circulations in Tibetan Plateau and surroundings. *Nat. Clim. Change* **2**, 663–667 (2012).
20. Dirnböeck, T., Essl, F. & Rabitsch, W. Disproportional risk for habitat loss of high-altitude endemic species under climate change. *Glob. Change Biol.* **17**, 990–996 (2011).
21. Schickhoff, U. et al. Do Himalayan treelines respond to recent climate change? An evaluation of sensitivity indicators. *Earth Syst. Dynam.* **6**, 245–265 (2015).
22. Singh, S., Sharma, S. & Dhyani, P. Himalayan arc and treeline: distribution, climate change responses and ecosystem properties. *Biodivers. Conserv.* **28**, 1997–2016 (2019).
23. Schickhoff, U. *The Upper Timberline in the Himalayas, Hindu Kush and Karakorum: A Review of Geographical and Ecological Aspects* (Springer, 2005).
24. Liang, E. et al. Species interactions slow warming-induced upward shifts of treelines on the Tibetan Plateau. *Proc. Natl Acad. Sci. USA* **113**, 4380–4385 (2016).
25. Lu, X. et al. Mountain treelines climb slowly despite rapid climate warming. *Glob. Ecol. Biogeogr.* **30**, 305–315 (2021).
26. Harsch, M. A., Hulme, P. E., McGlone, M. S. & Duncan, R. P. Are treelines advancing? A global meta-analysis of treeline response to climate warming. *Ecol. Lett.* **12**, 1040–1049 (2009).
27. Hansen, M. C. et al. High-resolution global maps of 21st-century forest cover change. *Science* **342**, 850–853 (2013).
28. Wan, Z. & Li, Z. A physics-based algorithm for retrieving land-surface emissivity and temperature from EOS/MODIS data. *IEEE Trans. Geosci. Remote Sens.* **35**, 980–996 (1997).
29. Fick, S. E. & Hijmans, R. J. WorldClim 2: new 1-km spatial resolution climate surfaces for global land areas. *Int. J. Climatol.* **37**, 4302–4315 (2017).
30. Breiman, L. Random forests. *Mach. Learn.* **45**, 5–32 (2001).
31. Venter, O. et al. Global terrestrial Human Footprint maps for 1993 and 2009. *Sci. Data* **3**, 160067 (2016).
32. Sigdel, S. R. et al. Moisture-mediated responsiveness of treeline shifts to global warming in the Himalayas. *Glob. Change Biol.* **24**, 5549–5559 (2018).
33. Dolezal, J. et al. Sink limitation of plant growth determines tree line in the arid Himalayas. *Funct. Ecol.* **33**, 553–565 (2019).
34. Dolezal, J. et al. Annual and intra-annual growth dynamics of *Myricaria elegans* shrubs in arid Himalaya. *Trees* **30**, 761–773 (2016).
35. Malcolm, J. R. et al. Global warming and extinctions of endemic species from biodiversity hotspots. *Conserv. Biol.* **20**, 538–548 (2006).
36. Ding, W., Ree, R. H., Spicer, R. A. & Xing, Y. Ancient orogenic and monsoon-driven assembly of the world's richest temperate alpine flora. *Science* **369**, 578–581 (2020).
37. Pirnat, J. Conservation and management of forest patches and corridors in suburban landscapes. *Landsc. Urban Plan.* **52**, 135–143 (2000).
38. Potapov, P. V. et al. Quantifying forest cover loss in Democratic Republic of the Congo, 2000–2010, with Landsat ETM plus data. *Remote Sens. Environ.* **122**, 106–116 (2012).
39. Paulsen, J. & Körner, C. GIS-analysis of tree-line elevation in the Swiss Alps suggests no exposure effect. *J. Veg. Sci.* **12**, 817–824 (2001).
40. FAO. *FRA 2000: On Definitions of Forest and Forest Change.* Forest Resource Assessment Programme Working Paper, Rome (Food and Agriculture Organization, 2000).
41. Luedeling, E., Siebert, S. & Buerkert, A. Filling the voids in the SRTM elevation model—a TIN-based delta surface approach. *ISPRS-J. Photogramm. Remote Sens.* **62**, 283–294 (2007).
42. Canny, J. Collision detection for moving polyhedra. *IEEE Trans. Pattern Anal. Mach. Intell.* **8**, 200–209 (1986).
43. More, J. J. & Sorensen, D. C. Computing a trust region step. *SIAM J. Sci. Comput.* **4**, 553–572 (1983).
44. Theobald, D. M., Harrison-Atlas, D., Monahan, W. B. & Albano, C. M. Ecologically-relevant maps of landforms and physiographic diversity for climate adaptation planning. *PLoS ONE* **10**, e0143619 (2015).
45. Hersbach, H. et al. The ERA5 global reanalysis. *Q. J. R. Meteorol. Soc.* **146**, 1999–2049 (2020).
46. Muñoz-Sabater, J. et al. ERA5-Land: a state-of-the-art global reanalysis dataset for land applications. *Earth Syst. Sci. Data* **13**, 4349–4383 (2021).
47. Liang, E., Wang, Y., Eckstein, D. & Luo, T. Little change in the fir tree-line position on the southeastern Tibetan Plateau after 200 years of warming. *New Phytol.* **190**, 760–769 (2011).
48. Anderegg, W. R. L. et al. Tree mortality predicted from drought-induced vascular damage. *Nat. Geosci.* **8**, 367–371 (2015).
49. Abatzoglou, J. T. et al. TerraClimate, a high-resolution global dataset of monthly climate and climatic water balance from 1958–2015. *Sci. Data* **5**, 170191 (2018).
50. Case, B. S. & Buckley, H. L. Local-scale topoclimate effects on treeline elevations: a country-wide investigation of New Zealand's southern beech treelines. *PeerJ* **3**, e1334 (2015).
51. Bush, M. B. et al. Fire and climate: contrasting pressures on tropical Andean timberline species. *J. Biogeogr.* **42**, 938–950 (2015).
52. Herrero, A., Zamora, R., Castro, J. & Hodar, J. A. Limits of pine forest distribution at the treeline: herbivory matters. *Plant Ecol.* **213**, 459–469 (2012).
53. Wang, Y. et al. The stability of spruce treelines on the eastern Tibetan Plateau over the last century is explained by pastoral disturbance. *For. Ecol. Manag.* **442**, 34–45 (2019).
54. Wei, Y. et al. Chinese caterpillar fungus (*Ophiocordyceps sinensis*) in China: current distribution, trading, and futures under climate change and overexploitation. *Sci. Total Environ.* **755**, 142548 (2021).
55. Miehe, G. et al. How old is the human footprint in the world's largest alpine ecosystem? A review of multiproxy records from the Tibetan Plateau from the ecologists' viewpoint. *Quat. Sci. Rev.* **86**, 190–209 (2014).
56. Willemann, R. J. & Storchak, D. A. Data collection at the international seismological centre. *Seismol. Res. Lett.* **72**, 440–453 (2001).
57. Chen, A., Huang, L., Liu, Q. & Piao, S. Optimal temperature of vegetation productivity and its linkage with climate and elevation on the Tibetan Plateau. *Glob. Change Biol.* **27**, 1942–1951 (2021).
58. Lehmkuhl, F. & Owen, L. A. Late Quaternary glaciation of Tibet and the bordering mountains: a review. *Boreas* **34**, 87–100 (2005).
59. Owen, L. A. & Dortch, J. M. Nature and timing of Quaternary glaciation in the Himalayan–Tibetan orogen. *Quat. Sci. Rev.* **88**, 14–54 (2014).
60. Strobl, C. et al. Conditional variable importance for random forests. *BMC Bioinform.* **9**, 307 (2008).
61. Zuur, A. F., Ieno, E. N. & Elphick, C. S. A protocol for data exploration to avoid common statistical problems. *Methods Ecol. Evol.* **1**, 3–14 (2010).
62. Vassallo, D., Krishnamurthy, R. & Fernando, H. J. S. Decreasing wind speed extrapolation error via domain-specific feature extraction and selection. *Wind Energy Sci.* **5**, 959–975 (2020).
63. Ramirez-Villegas, J. & Jarvis, A. *Downscaling Global Circulation Model Outputs: The Delta Method Decision and Policy Analysis* Working Paper No. 1 (CIAT, 2010).
64. Wu, Z. & Raven, P. *Flora of China* (Science Press and Missouri Botanical Garden Press, 1994–2006).
65. Wu, Z. *Flora of Tibet* (Science Press, 1987).
66. Maclean, I. M. D. et al. Microclimates buffer the responses of plant communities to climate change. *Glob. Ecol. Biogeogr.* **24**, 1340–1350 (2015).
67. Randin, C. F. et al. Climate change and plant distribution: local models predict high-elevation persistence. *Glob. Change Biol.* **15**, 1557–1569 (2009).

68. Scherrer, D. & Körner, C. Topographically controlled thermal-habitat differentiation buffers alpine plant diversity against climate warming. *J. Biogeogr.* **38**, 406–416 (2011).

Acknowledgements

We thank C. Körner for his constructive suggestions and edits to the text. We also thank F. Zhuang and Y. Wang for helping with endemic species identification. This study was supported by the Second Tibetan Plateau Scientific Expedition and Research Program (2019QZKK0405), the National Natural Science Foundation of China (41922004), the NSFC project Basic Science Centre for Tibetan Plateau Earth System (41988101-04), the Preliminary Research on Three Poles Environment and Climate Change (2019YFC1509103) and the Key Research and Development Programs for Global Change and Adaptation (2017YFA0603604). We also acknowledge the support of Kathmandu Center for Research and Education, Chinese Academy of Sciences—Tribhuvan University.

Author contributions

T.W. and Z.S. designed the research. T.W. and X.W. wrote the paper. X.W. and J.X. performed the data analysis. J.X. and X.W. manually interpreted realized upper range limit of trees using Google Earth images. Y.Y. led identification of alpine endemic species. A.C., S.W., E.L. and S.P. contributed to the interpretation of the results and to the text.

Competing interests

The authors declare no competing interests.

Additional information

Extended data is available for this paper at https://doi.org/10.1038/s41559-022-01774-3.

Supplementary information The online version contains supplementary material available at https://doi.org/10.1038/s41559-022-01774-3.

Correspondence and requests for materials should be addressed to Tao Wang.

Peer review information *Nature Ecology & Evolution* thanks the anonymous reviewers for their contribution to the peer review of this work.

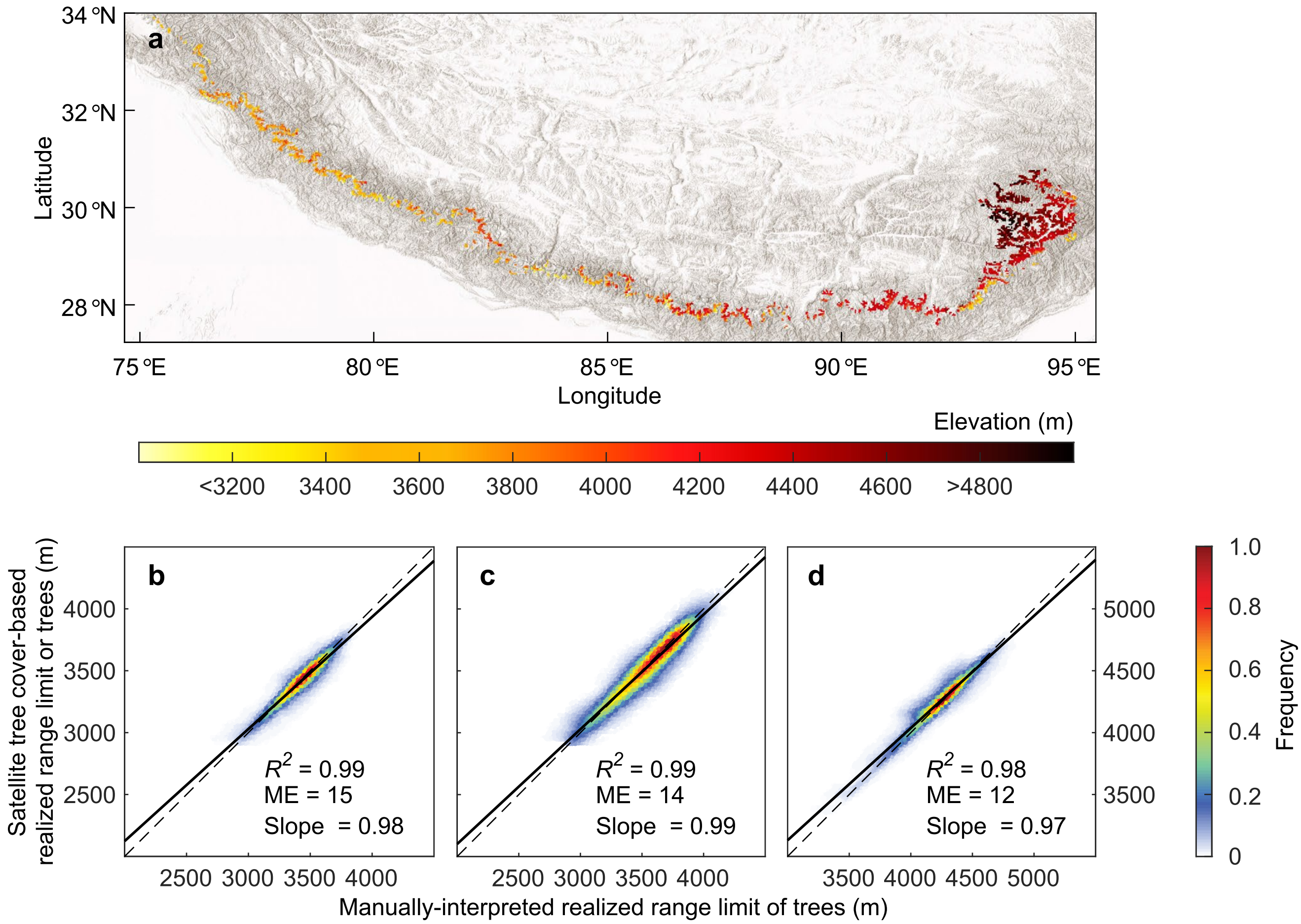

Extended Data Fig. 1 | Validation of satellite tree-cover-based realized range limit of trees against manual interpretation from Google Earth high-resolution images over the Himalaya. (a) The elevational distribution of manually interpreted realized range limit of trees from Google Earth high-resolution images. The relationships of satellite tree-cover-based realized range limit of trees with manual interpretation in western (b), central (c) and eastern regions (d), with the 1:1 line (dashed) and the regression line (continuous). R^2 and ME indicate the coefficient of determination and the mean error, respectively.

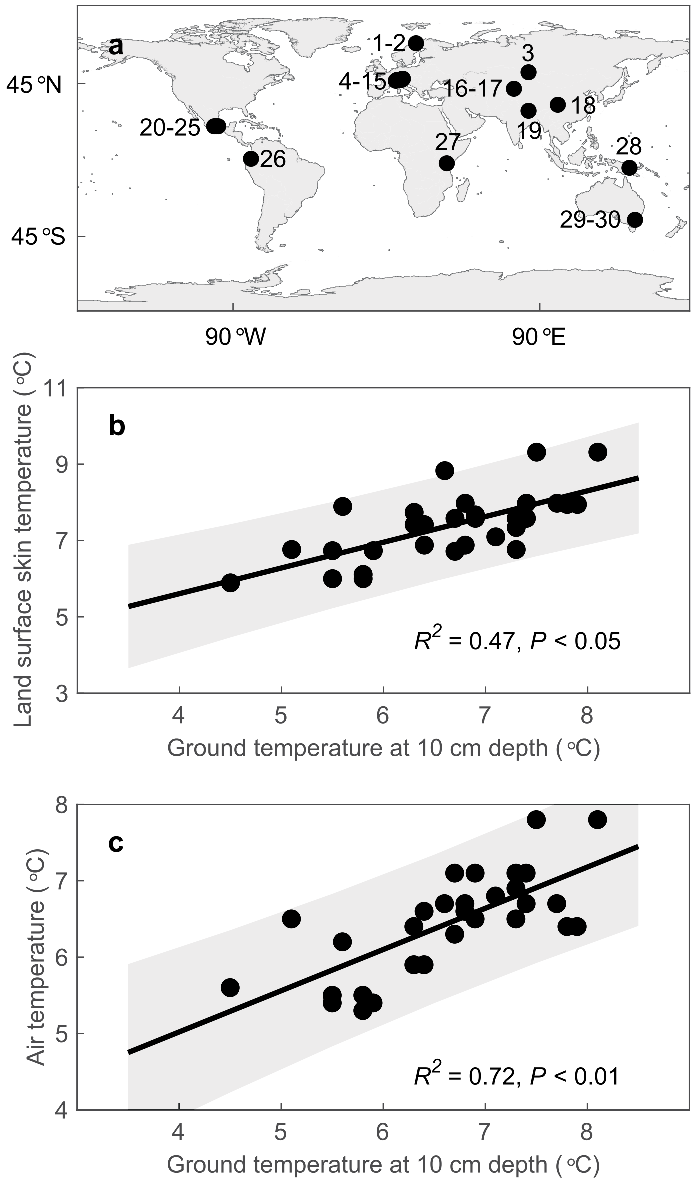

Extended Data Fig. 2 | Linking ground temperature at 10 cm depth with the land surface skin temperature and air temperature at thermal treeline sites. (a) The global distribution of thermal treeline sites with a record of the soil temperature at a depth of 10 cm. (b-c) The regression between growing-season land surface skin temperature (°C) (b), air temperature (°C) (c), and ground temperature (°C) across sites, with the grey shading indicates 95% confidence intervals. The land surface skin temperature at each site is taken from Collection 6 of the Moderate Resolution Imaging Spectroradiometer at a spatial resolution of 1 km.

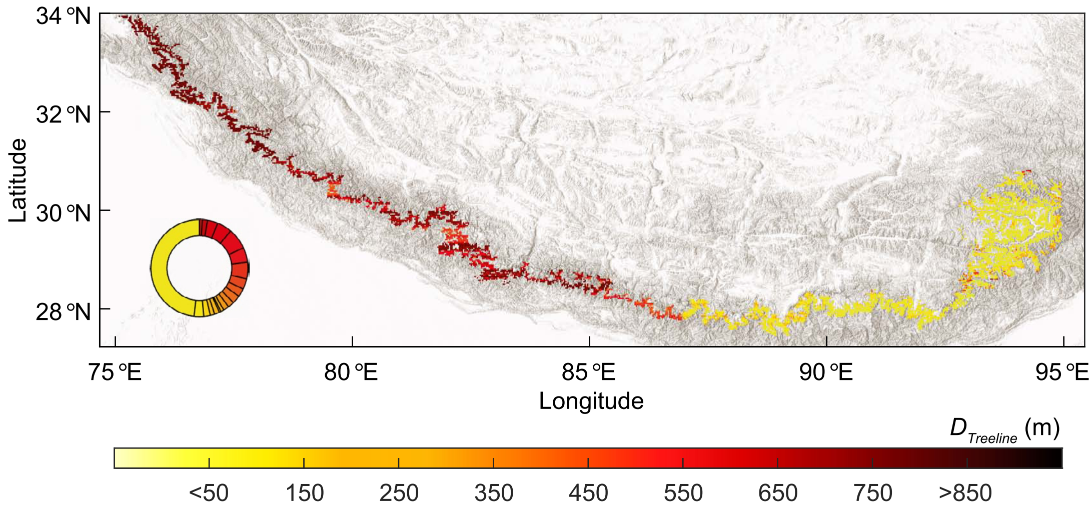

Extended Data Fig. 3 | Spatial distribution of derivation of realized range limit of trees from treeline elevation ($D_{Treeline}$) across the Himalayas. The insects show the frequency distribution of $D_{Treeline}$.

nature portfolio

Corresponding author(s): Tao Wang

Last updated by author(s): Mar 23, 2022

Reporting Summary

Nature Portfolio wishes to improve the reproducibility of the work that we publish. This form provides structure for consistency and transparency in reporting. For further information on Nature Portfolio policies, see our Editorial Policies and the Editorial Policy Checklist.

Statistics

For all statistical analyses, confirm that the following items are present in the figure legend, table legend, main text, or Methods section.

n/a	Confirmed	
☐	☒	The exact sample size (*n*) for each experimental group/condition, given as a discrete number and unit of measurement
☐	☒	A statement on whether measurements were taken from distinct samples or whether the same sample was measured repeatedly
☐	☒	The statistical test(s) used AND whether they are one- or two-sided *Only common tests should be described solely by name; describe more complex techniques in the Methods section.*
☐	☒	A description of all covariates tested
☐	☒	A description of any assumptions or corrections, such as tests of normality and adjustment for multiple comparisons
☐	☒	A full description of the statistical parameters including central tendency (e.g. means) or other basic estimates (e.g. regression coefficient) AND variation (e.g. standard deviation) or associated estimates of uncertainty (e.g. confidence intervals)
☐	☒	For null hypothesis testing, the test statistic (e.g. *F*, *t*, *r*) with confidence intervals, effect sizes, degrees of freedom and *P* value noted *Give P values as exact values whenever suitable.*
☐	☒	For Bayesian analysis, information on the choice of priors and Markov chain Monte Carlo settings
☐	☒	For hierarchical and complex designs, identification of the appropriate level for tests and full reporting of outcomes
☐	☒	Estimates of effect sizes (e.g. Cohen's *d*, Pearson's *r*), indicating how they were calculated

Our web collection on statistics for biologists contains articles on many of the points above.

Software and code

Policy information about availability of computer code

Data collection	Google Earth
Data analysis	The analyses and mapping were performed using MATLAB (R2018b), R (3.6.1) and ArcGIS 10.2.

For manuscripts utilizing custom algorithms or software that are central to the research but not yet described in published literature, software must be made available to editors and reviewers. We strongly encourage code deposition in a community repository (e.g. GitHub). See the Nature Portfolio guidelines for submitting code & software for further information.

Data

Policy information about availability of data

All manuscripts must include a data availability statement. This statement should provide the following information, where applicable:

- Accession codes, unique identifiers, or web links for publicly available datasets
- A description of any restrictions on data availability
- For clinical datasets or third party data, please ensure that the statement adheres to our policy

All data is available in the main text or the supplementary information. The spatial distribution of manually-interpreted and Landsat tree-cover derived realized range limit of trees can be accessed through https://globalmapping.users.earthengine.app/view/realized-upper-range-limit-position-over-himalaya.
All computer codes used in this study can be provided by the corresponding author upon reasonable requests.

Field-specific reporting

Please select the one below that is the best fit for your research. If you are not sure, read the appropriate sections before making your selection.

☐ Life sciences ☐ Behavioural & social sciences ☒ Ecological, evolutionary & environmental sciences

For a reference copy of the document with all sections, see nature.com/documents/nr-reporting-summary-flat.pdf

Ecological, evolutionary & environmental sciences study design

All studies must disclose on these points even when the disclosure is negative.

Study description	We used 30-m resolution tree-cover data from the Landsat satellite to map the realized upper range limit of tree positions and uncover habitat loss of the Himalayan endemic flora driven by warming-forced upward shift of the trees.
Research sample	We used the 30-m resolution tree cover database derived from Google Earth engine. Hansen, M. C. et al., (2013). High-Resolution Global Maps of 21st-Century Forest Cover Change. Science 342, 850–853. All data needed to evaluate the conclusions in this paper are present in the paper and/or the Supplementary Information.
Sampling strategy	N/A
Data collection	We collect more than 0.7 million manually-interpreted realized range limit elevation samples from Google Earth images. We also compiled a list of in situ measurements by reviewing the prior literature.
Timing and spatial scale	We used tree-cover data circa 2015 across Himalaya.
Data exclusions	N/A
Reproducibility	N/A
Randomization	N/A
Blinding	N/A

Did the study involve field work? ☐ Yes ☒ No

Reporting for specific materials, systems and methods

We require information from authors about some types of materials, experimental systems and methods used in many studies. Here, indicate whether each material, system or method listed is relevant to your study. If you are not sure if a list item applies to your research, read the appropriate section before selecting a response.

Materials & experimental systems

n/a	Involved in the study	
☒	☐	Antibodies
☒	☐	Eukaryotic cell lines
☒	☐	Palaeontology and archaeology
☒	☐	Animals and other organisms
☒	☐	Human research participants
☒	☐	Clinical data
☒	☐	Dual use research of concern

Methods

n/a	Involved in the study	
☒	☐	ChIP-seq
☒	☐	Flow cytometry
☒	☐	MRI-based neuroimaging